J. Fluid Mech. (1987), *vol.* 177, *pp.* 83–107
Printed in Great Britain

On the role of subharmonic perturbations in the far wake

By E. MEIBURG†
Institut fur Theoretische Strömungsmechanik, DFVLR, D-3400 Göttingen, West Germany

(Received 16 April 1986)

The possibility of an excitation of individual subharmonic perturbations in each of the shear layers forming the far wake is investigated numerically. Principal considerations allow for the existence of two equivalent subharmonic modes which by opposite routes can lead to a doubling of the wavelength in the wake. Since vortical disturbances in the far wake are amplified only convectively, the simultaneous existence of both modes in the flow field is possible, which could provide an explanation for the group structure observed experimentally in the far wake. These considerations also provide a logical explanation of the finding of a very regular vortex pairing process in forced wakes.

Two-dimensional numerical simulations assuming incompressible flow and almost inviscid dynamics illustrate the opposite developments of regions dominated by the two different modes and also confirm the possibility of a resulting group structure. As an important result it is demonstrated that, if vortex pairing plays an important role in the growth of the far-wake structure, this does not have to be related to the excitation of the subharmonic peak in the frequency spectrum. Quite the contrary, it is to be expected that the subharmonic itself is of minor importance and that instead a small frequency and its multiples related to the group structure of the flow dominate the spectrum. In the light of these considerations measurements by Cimbala (1984) are discussed and frequency spectra recorded by him are analysed more closely. Various properties of these spectra seem to indicate that vortex pairing might be significant with respect to the evolution of the far-wake structure.

1. Introduction

The breakdown of the Kármán vortex street and the subsequent formation of a secondary vortex street were first observed by Taneda (1959). He found the ratio of the lengthscales of the secondary and the primary street to lie between 1.8 and 10, depending on the Reynolds number. Other experimentalists have confirmed these observations, and two different explanations for the mechanism causing the breakdown and the subsequent reordering have emerged. One of them attributes this process to vortex pairing, which has long been recognized as the mechanism responsible for the growth of single shear layers (Winant & Browand 1974). Matsui & Okude (1983) presented experimental evidence for the natural occurrence of vortex pairing in wake flows and they also demonstrated that forcing of the wake with one-half or one-third of the shedding frequency results in very regular pairings of the individual vortices on each side of the wake. The calculations of Aref & Siggia (1981)

† Present address: Department of Chemical Engineering, Stanford University, Stanford, CA 94305, USA.

also show the possibility of pairing in a Kármán vortex street. They describe the evolution of a metastable vortex street which after a long time goes unstable and 'breaks down'. During this process individual vortex structures can undergo pairings.

The other explanation for the evolution of the far-wake structure is based on linear stability considerations of the time-averaged wake velocity profile. Viscous effects as well as changes in the average wake profile in the streamwise direction, which damp waves that had been amplified further upstream, are held responsible for the disappearance of the Kármán vortex street. The maximum amplification shifts to longer waves in the streamwise direction, which in turn leads to the formation of the secondary street. Among others, Cimbala (1984) concludes from his experimental observations and stability calculations that this explanation is adequate for the generation of the far-wake structure. He found the energy spectrum to contain discrete peaks in the far wake, but in most cases the subharmonic frequency did not seem to play a prominent role, which he interprets as evidence against a pairing growth mechanism. On the other hand, his figure 6.3 seems to demonstrate a certain sensitivity of the wake flow to subharmonic disturbances. Cimbala's measurements also confirm earlier findings by Townsend (1979), who observed a group structure of the secondary vortex street. The frequency is fixed within each group but can vary from one group to the next, i.e. a time record of a velocity fluctuation will show a single main frequency followed by a transition to a different frequency. A possible relation between this group phenomenon and the emergence of further frequencies besides the shedding frequency is discussed by Sirovich (1985).

In the following, we attempt an explanation of the apparent discrepancy between the observation by Matsui & Okude of a very regular vortex pairing process in the forced wake and the measurements by Cimbala which do not indicate a special importance of the subharmonic frequency itself. We will present a new model for the growth mechanism of the wake which provides an explanation for many of the observations of both authors. It is suggested that each of the shear layers forming the wake is able to amplify individual subharmonic perturbations, similarly to the well-known behaviour of a single shear layer. As a consequence of the interaction of the two shear layers, this gives rise to the existence of two subharmonic modes for the wake flow, which could dominate different parts of the flow field in an alternating fashion. This mechanism then also provides an explanation for the observed group structure mentioned above as well as for some of the effects found in the numerical simulations by Aref & Siggia (1981).

In §2 we will, after a brief reference to the single shear layer, discuss the possibility of an amplification of individual subharmonic perturbations in the two opposite shear layers forming the Kármán vortex street. The impact of these perturbations on the interaction of the two sides of the vortex street will be analysed qualitatively, and it will be shown that they cause the vortex street to develop asymmetrically. Furthermore, it will be demonstrated that two different subharmonic modes are possible, each of which is related to a certain combination of the phase angles of the individual subharmonic perturbations of the shear layers.

In order to investigate the nonlinear behaviour of the flow field, we simulated the evolution of two opposite shear layers numerically for various initial conditions. The results will be presented in §3. The numerical technique used for these simulations discretizes the vorticity field, an approach that had been used before for the analysis of wake flows by various authors, among them Aref & Siggia (1981). Leonard (1980, 1985) gives a general overview of these vortex methods. The algorithm applied here

treats the temporally developing case, i.e. the flow is considered periodic in streamwise direction. It furthermore assumes two-dimensional, incompressible and almost inviscid dynamics.

The various sets of initial conditions for which simulations have been carried out include cases where only one mode is present in the flow field, as well as cases containing both modes. The effect on both the evolution of the structure of the vortex street and the corresponding frequency spectra will be demonstrated. It will be shown how the presence of two subharmonic modes in the flow field can result in the cancellation of the subharmonic peak in the frequency spectrum.

Finally, in §4 a discussion of the numerical results will be given. We will compare our numerically generated frequency spectra with the spectra recorded by Cimbala (1984) and reinterpret those in the light of our proposed model for the growth mechanism of the wake flow. The relation of our findings to experimental and theoretical observations of other authors will also be demonstrated, followed by a discussion of possible effects of viscosity and three-dimensionality, which are not included in the present numerical simulations.

2. Influence of the phase angle of the subharmonic perturbation

Let us first consider the single shear layer. A sinusoidal perturbation of wavelength 2π of the initially parallel flow leads to the onset of the Kelvin–Helmholtz instability mechanism, which causes a roll-up into large-scale vortices. Among all phase angle values for waves with twice the wavelength of the basic disturbance (subharmonic waves), two phases, shown in figures 1 and 2, are of special importance (see Patnaik, Sherman & Corcos 1976; Riley & Metcalfe 1980; Corcos & Sherman 1984). If we define the reference point $x = x_0$ as the location of one of the vortices generated by the initial Kelvin–Helmholtz instability we can identify these two subharmonic waves $y_2(x)$ as having a phase difference $\Delta\phi$ with respect to the basic wave $y_1(x)$ of an odd or even number of multiples of $\frac{1}{2}\pi$, respectively. Here $y_1(x)$ and $y_2(x)$ can be thought of as wavy dislocations of the initially straight vorticity layers related to the parallel shear flow. If at x_0 the subharmonic wave has a phase difference of an odd number of multiples of $\frac{1}{2}\pi$ with respect to the basic wave (figure 1), i.e. if it has its maxima and minima at the positions where the basic wave has its strongest gradients, it will alternately shift the evolving vortices up and down without changing their strength. This results in the vortices rotating around each other and finally in their merging or pairing. If, on the other hand, the phase difference is an even number of multiples of $\frac{1}{2}\pi$, the subharmonic will alternately strengthen and weaken the vortices without shifting their centres (figure 2). The stronger vortices will now 'shred' the weaker ones, which finally also leads to the doubling of the basic wavelength.

Experimental observations as well as calculations (Riley & Metcalfe 1980; Corcos & Sherman 1984) indicate that in the single layer subharmonic waves with a phase difference of an odd number of multiples of $\frac{1}{2}\pi$ experience a stronger amplification. Consequently, in the following discussion of the amplification of subharmonic waves in the shear layers forming the wake we will confine ourselves to these subharmonic waves exclusively, although our analysis would also be valid in principle for other subharmonic waves.

Let us now analyse two opposite shear layers disturbed with the same basic wave of length 2π, thus developing into two staggered vortex rows. Suppose each of them contains individual subharmonic perturbations of the above kind. If the shear layers

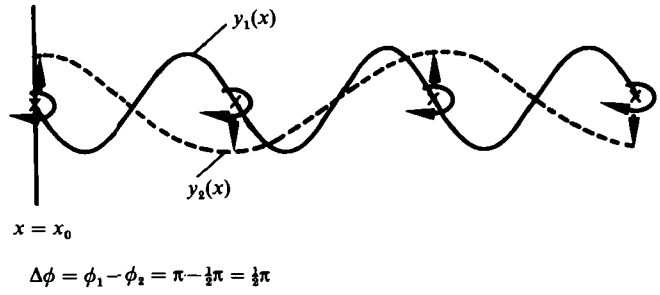

FIGURE 1. If the phase difference $\Delta\phi$ of the basic wave $y_1(x)$ and the subharmonic wave $y_2(x)$ at $x = x_0$ is an odd number of multiples of $\frac{1}{2}\pi$ the vortices will alternately be shifted up and down as indicated by the straight arrows. This will lead to the pairing of the individual vortices.

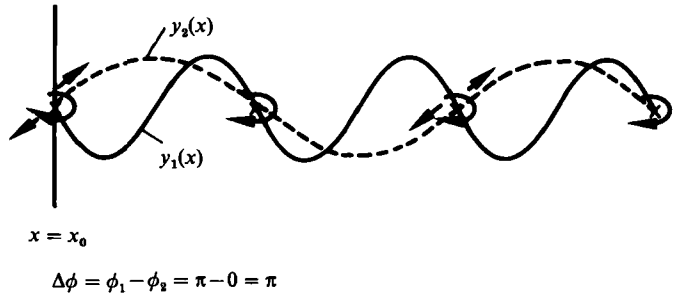

FIGURE 2. If the phase difference $\Delta\phi$ of the basic wave $y_1(x)$ and the subharmonic wave $y_2(x)$ at $x = x_0$ is an even number of multiples of $\frac{1}{2}\pi$ the vortices will alternately be strengthened and weakened. This will lead to a period doubling through the shredding of the weaker vortices in the strain field of the stronger ones as indicated by the arrows.

are far apart, they will only weakly interact and each of them will undergo a pairing transition, as shown by the calculations of Aref & Siggia (1981). The interaction becomes stronger as the distance between the layers decreases. Aref & Siggia find a critical ratio of the distance between the layers and the distance between the vortices in each layer of about 0.6, below which the individual vortices do not pair but instead form a metastable Kármán vortex street. Their calculations show that after a long time this vortex street is unstable and 'breaks down'. During this process vortices can pair or form neutral dipoles. These observations indicate that the growth of individual subharmonic disturbances within each of the shear layers does not abruptly diminish to zero but may only slightly decrease as the interaction between the opposite shear layers becomes more significant.

It now becomes obvious that, if the two staggered rows of vortices forming the Kármán vortex street can have individual subharmonic disturbances $y_{2t}(x)$ and $y_{2b}(x)$, respectively, with a phase difference of an odd number of multiples of $\frac{1}{2}\pi$ with respect to the basic wave $y_1(x)$ at the respective reference points x_{0t} and x_{0b}, two different modes can appear (figure 3). If in the upper row the subharmonic perturbation $y_{2t}(x)$ has a phase difference $\Delta\phi_t$ of $\frac{1}{2}\pi$, the subharmonic disturbance $y_{2b}(x)$ in the lower row can take values for the phase difference $\Delta\phi_b$ of $\frac{1}{2}\pi$ (figure 3*a*, mode A) or $-\frac{1}{2}\pi$ (figure 3*b*, mode B), each of them leading to a different development

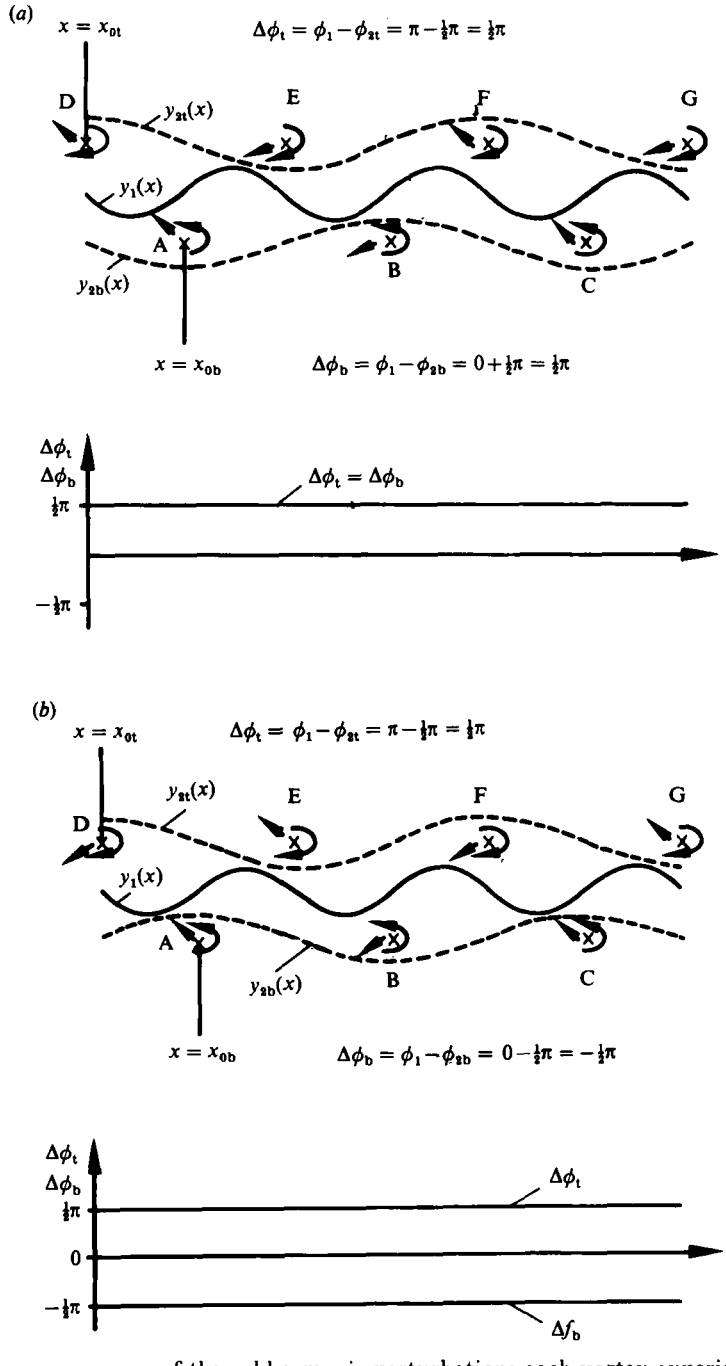

FIGURE 3. As a consequence of the subharmonic perturbations each vortex experiences a change in the relative impact of its two closest neighbours in the opposite row. This change induces a differential velocity, which is qualitatively indicated by the straight arrows. (*a*) Mode A: the phase difference between the subharmonic (– – –) and the basic wave (——) in both layers is $\frac{1}{2}\pi$ at the respective reference points. The differential velocities induced by this configuration amplify the subharmonic perturbation in the upper row whereas in the lower row they slow its growth down. (*b*) Mode B: here the phase difference between the subharmonic (– – –) and the basic (——) wave in the upper layer is $\frac{1}{2}\pi$ whereas in the lower layer it is $-\frac{1}{2}\pi$. This configuration tends to amplify the growth of the subharmonic in the lower row and to damp it in the upper row.

of the vortex street, as explained below. Here the respective reference points have been defined to be the centre of the leftmost vortex x_{0t} for the upper layer; the reference point for the lower layer x_{0b} then is the centre of the vortex in the lower row that follows to the right. For mode A (figure 3*a*) the subharmonic perturbation $y_{2t}(x)$ indicated by the dashed wavy line in the upper row tends to shift vortices D and F up so that their influence on the vortices of the lower row decreases, whereas E and G are brought closer to the opposite layer which causes their influence on it to increase. The subharmonic disturbance in the lower layer $y_{2b}(x)$ plays a corresponding role there. If we now analyse the impact of the subharmonic perturbations of the neighbouring regions of both rows on, say, vortex E, we find that B has gained some influence on E since it has moved closer to E whereas the impact of A on E remains constant to a first approximation. This will induce a small differential velocity on E indicated by the arrow. If we carry out a corresponding analysis for all of the vortices we find that the induced velocities tend to amplify the subharmonic wave in the upper row, whereas the subharmonic perturbation of the lower row is being damped. This in turn will lead to an unsymmetrical development of the vortex street, causing the upper row of vortices to develop a subharmonic character faster than the lower one.

The disturbances described above are of a different nature than those on which von Kármán based his stability analysis of two staggered rows of point vortices (see, e.g., Lamb 1932). While von Kármán treated the configuration of point vortices as one system which he perturbed with a single wave, we look at the flow as consisting of two separate but interacting rows of vortices, each of which can amplify individual disturbances. It would be of interest to carry out a stability analysis for the latter type of perturbations corresponding to the classical one that von Kármán presented, and to compare the relative growth rates. Especially in the light of the findings of Meiron, Saffman & Schatzman (1984), that giving the vortices of a Kármán vortex street a finite core size does not change the stability characteristics drastically, a study along those lines could provide some information about how the linear growth rates of the perturbations examined in this paper compare to those studied previously. However, since the ultimate goal of this paper is to investigate the nonlinear evolution of a smooth velocity profile, the above qualitative argument concerning the stability of rows of concentrated vortices appears sufficient at this point and the quantitative linear analysis of the corresponding point-vortex configuration is left to future work.

A corresponding analysis for mode B (figure 3*b*) demonstrates that, if the subharmonic wave in the lower layer $y_{2b}(x)$ is shifted by one basic wavelength compared with mode A, the opposite development will take place, and the subharmonic perturbation of the lower row will now be amplified. From this analysis follows the possibility of the existence of two equally probable subharmonic modes for the wake flow which cause opposite developments of the vortex street. It should be mentioned that case A can be transformed into case B by shifting the whole flow field by half a basic wavelength in the flow direction and then rotating it around the centreline of the wake.

From the above we can conclude that, if individual subharmonic perturbations are excited within each of the two shear layers of the wake, there are two modes that can be identified by the phase difference $\Delta\phi_s = \Delta\phi_t - \Delta\phi_b$ of the subharmonic perturbations in the upper and lower rows, respectively, and that lead to an unsymmetrical development of the wake:

Mode	$\Delta\phi_t$	$\Delta\phi_b$	$\Delta\phi_s = \Delta\phi_t - \Delta\phi_b$
A	$\frac{1}{2}\pi$	$\frac{1}{2}\pi$	0
	$-\frac{1}{2}\pi$	$-\frac{1}{2}\pi$	0
B	$\frac{1}{2}\pi$	$-\frac{1}{2}\pi$	π
	$-\frac{1}{2}\pi$	$\frac{1}{2}\pi$	$-\pi$

This takes us to the question of how the structure of the far wake might be determined in a real flow if individual subharmonic perturbations on each side of the wake play an important role. One could imagine that a random subharmonic disturbance might be amplified initially and then influence the whole flow field including the upstream region, thus locking the whole flow into one mode. However, as Koch (1985) has shown, linear vortical disturbances are amplified only convectively in the far wake, which means that they are damped in the upstream direction. Thus, at least within the frame of linearized theory, a single spatially and temporally confined disturbance in the far wake cannot cause the whole flow to lock into one mode, and so an alternating appearance of the two modes seems possible.

In the following, two-dimensional vortex-street simulations for selected initial perturbations are presented. The consequences of the appearance of two different subharmonic modes with respect to the formation of the far-wake structure and the corresponding frequency spectra will be investigated.

3. Two-dimensional numerical simulations of wake flows for selected initial disturbances

Two-dimensional calculations using a discrete-vortex method were performed in order to illustrate the nonlinear development of wake flows for selected initial disturbances. We confine ourselves to the case of a temporally amplified flow, because this allows us to assume periodic boundary conditions in the streamwise direction. This approach appears to be legitimate since the flow conditions in the far wake vary slowly, which means that we deal with slowly growing perturbations of a base flow that does not undergo rapid changes in the streamwise direction. Far away from the centre of the wake we assume potential flow. The numerical technique is based on the Biot–Savart integral

$$\boldsymbol{u}(\boldsymbol{x}) = -\frac{1}{4\pi}\int \frac{(\boldsymbol{x}-\boldsymbol{x}')\times\boldsymbol{\omega}(\boldsymbol{x}')}{|\boldsymbol{x}-\boldsymbol{x}'|^3}\,\mathrm{d}V(\boldsymbol{x}') + \boldsymbol{u}_{\mathrm{pot}}(\boldsymbol{x}),$$

which, for incompressible flow fields, enables us to calculate the velocity $\boldsymbol{u}$ at a given point $\boldsymbol{x}$ by integrating over the vorticity field and adding the potential-velocity component. Initially, each of the two shear layers is represented by a row of two-dimensional discrete vortex blobs with finite core radius σ (figure 4). The finite core size results in a smooth distribution of the vorticity and thus avoids the singularity associated with the fact that for point vortices the distribution function of the vorticity has the shape of a δ-function. It requires the specification of a distribution function of the vorticity ω (a scalar in two dimensions) over the core radius r. In the present simulation, we employed

$$\frac{\omega(r)}{\Gamma} = \frac{\alpha}{\pi\sigma^2}\frac{1}{\left(\frac{r^2}{\sigma^2}+\alpha\right)^2},$$

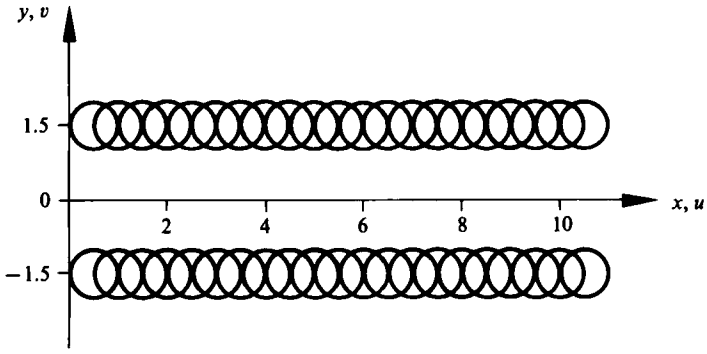

FIGURE 4. For the numerical simulations, the two sides of the average wake profile are represented by rows of vortex blobs which are perturbed at the beginning of the simulation.

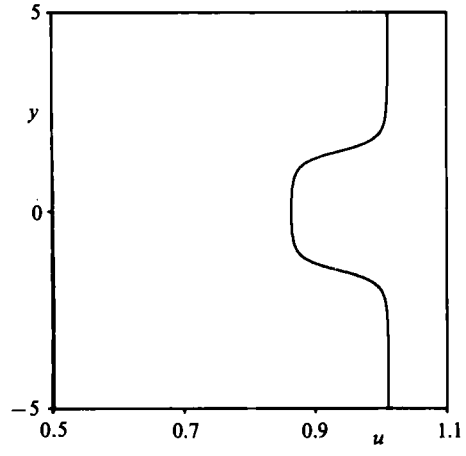

FIGURE 5. The velocity profile represented by the initial configuration of the discrete vortex blobs.

where $\alpha = 0.413$, as suggested by Leonard (1980). Assuming inviscid dynamics, the velocity of vortex blob i located at $\boldsymbol{x}_i$ can then be evaluated according to the Biot–Savart integral by summing the velocities that all other vortex blobs in the flow field with the respective circulations Γj induce on blob i:

$$u(\boldsymbol{x}_i) = -\frac{1}{2\pi} \sum_{\substack{j=1 \\ j \neq 1}}^{N} \frac{y_i - y_j}{(x_i - x_j)^2 + (y_i - y_j)^2 + \alpha} * \Gamma_j,$$

$$v(\boldsymbol{x}_i) = \frac{1}{2\pi} \sum_{\substack{j=1 \\ j \neq 1}}^{N} \frac{x_i - x_j}{(x_i - x_j)^2 + (y_i - y_j)^2 + \alpha} * \Gamma_j,$$

where N is the total number of vortex blobs in the flow field.

Initially, the centres of the vortex blobs are about 0.125 core radii apart, so they have considerable overlap and form a smooth vorticity distribution. At the beginning of the calculation, the two rows of vortex blobs are perturbed by periodic dislocations of the blob centres in the transverse direction. From then on, the nonlinear development of the flow is calculated by evaluating the velocities of the vortex blobs at each time step and advancing them over a finite time step using a second-order predictor–corrector integration scheme

Simulation	Mode A	Mode B
I	entire flow field	—
II	—	entire flow field
III	$x = 25.13$ to 75.40	$x = 100.53$ to 150.80
IV	$x = 0$ to 50.27	$x = 75.40$ to 125.66
	$x = 226.19$ to 276.46	$x = 150.80$ to 201.06

TABLE 1. The main features of the four wake-flow simulations

$$x' = x(t) + u(x, t) * \Delta t,$$

$$x(t + \Delta t) = x(t) + 0.5 * (u(x, t) + u'(x')) * \Delta t.$$

At the beginning of the simulation, the perturbation of the base flow is small, which allows us to start with a large time-step. During the calculation, the time-step is continuously being reduced, according to the criterion that the difference in the velocities obtained for a vortex at the predictor step and the corrector step, respectively, multiplied with the actual time-step should never exceed 2 % of the core radius of the blobs. This criterion was established during test calculations and has proven reliable in reducing the time-step when local acceleration effects increase. The core size and the shape of the vortex blobs were left unchanged throughout the simulation, i.e. the effect of the local strain field on the form of the vortex core was neglected. Discretization errors appearing in the course of the numerical integration perturb the flow in addition to the initially imposed disturbances and can cause wavelengths other than the initially introduced ones and their harmonics to be excited as well.

At the beginning of the simulation, the shear layers have a transverse separation of 3 unit lengths, the unit length being the diameter of the vortex blobs. This, together with a potential-velocity component in the form of a uniform parallel flow of unit velocity 1, results in the initial undisturbed wake profile depicted in figure 5. The velocity defect depends on the circulation per unit length of the shear layers. The basic wavelength is 2π in all calculations. The ratio of the distance between the two layers and the streamwise wavelength comes to 0.48 and lies well within the regime in which Aref & Siggia (1981) observed the formation and subsequent breakdown of vortex streets. Unless otherwise stated, the amplitude of the initial wavy perturbations is 0.1, which is small compared to the distance between the layers. Comparisons carried out for a test case have shown that an initial amplitude of 0.01 yields qualitatively the same results. Time is non-dimensionalized with the unit length and the free-stream velocity. The time-step is taken as 10 initially and is then reduced by about two orders of magnitude in the course of the simulation. The flow fields are visualized by means of contour plots of the vorticity distribution as well as by frequency spectra. These are obtained by analysing the flow field at a fixed time and Fourier transforming the v-velocity signal at the arbitrarily chosen y-coordinate of 1.8 for a large number of x-positions. In order to facilitate the interpretation of the spectra, all frequencies are normalized with the frequency of the basic wave and all amplitudes are referred to the highest one. From these spectra we can determine the relative amplification of the various wavelengths.

We have carried out a total of four simulations, the main features of which are listed in table 1.

Let us first consider the results obtained from simulation I in which each shear layer

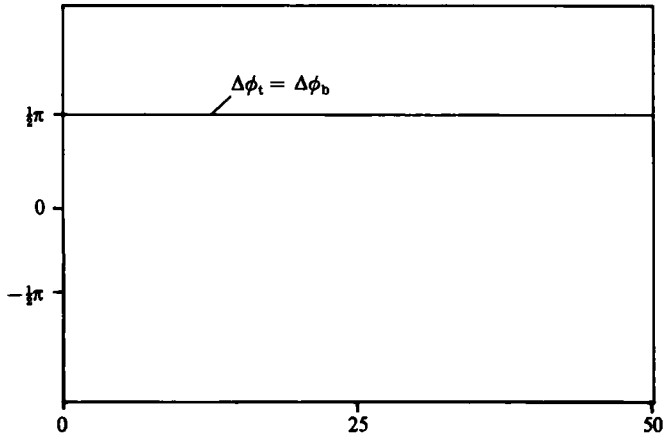

FIGURE 6. The phase relations of the subharmonic perturbations in the upper and the lower layer *vs.* the streamwise coordinate (simulation I).

is initially disturbed by the same basic wave and in addition has an individual subharmonic perturbation which is the same over the entire length of the control volume (figure 6). This means that of the two subharmonic modes described above only one mode is present; for simulation I this is mode A. The control volume contains eight basic wavelengths, and each layer is discretized into 765 vortex blobs. At the beginning of the simulation the amplitudes of the basic and the subharmonic perturbations are equal. During the initial stages the basic wavelength experiences a stronger amplification which causes its peak to dominate the frequency spectrum at $t = 34.4$ (figure 7). It is obvious that, owing to the interaction of the layers, the subharmonic perturbation is initially amplified more strongly in the upper layer, whereas it is damped in the lower one (figure 8). The nonlinear development later causes a reversal and the subharmonic then grows faster in the lower layer. We see that the pairing process, which is clearly visible from the vorticity plots, proceeds at different speeds on both sides of the wake. We consider it to be completed when the vorticity contour plots show only one maximum of the vorticity distribution instead of two. In the lower layer this has happened by $t = 471.9$, whereas in the upper layer it takes until about $t = 596.9$. From the energy spectrum we recognize that, after initially dominating the flow, the relative energy contained in the basic wavelength continuously decreases towards the end of the simulation, whereas the subharmonic peak increases. We further observe that, due to discretization errors that occur in the process of integration, wavelengths other than those introduced at the beginning and their harmonics are also being excited. These waves present harmonics of the longest possible waves having the length of the control volume.

Next consider a configuration (simulation II) that initially is identical with the previous one except for the subharmonic perturbation of the lower layer which has been shifted by one basic wavelength (figure 9). This means that now mode B dominates throughout the entire flow field. As should be expected from the reasons given above the wake now develops in a manner opposite to the case just described, as shown in figures 10 and 11. The subharmonic disturbance is at first amplified more strongly in the lower layer, and later the pairing proceeds faster in the upper layer (figure 11). Only discretization errors can cause other wavelengths than those in simulation I to be amplified, as can be seen from the frequency spectrum (figure 10).

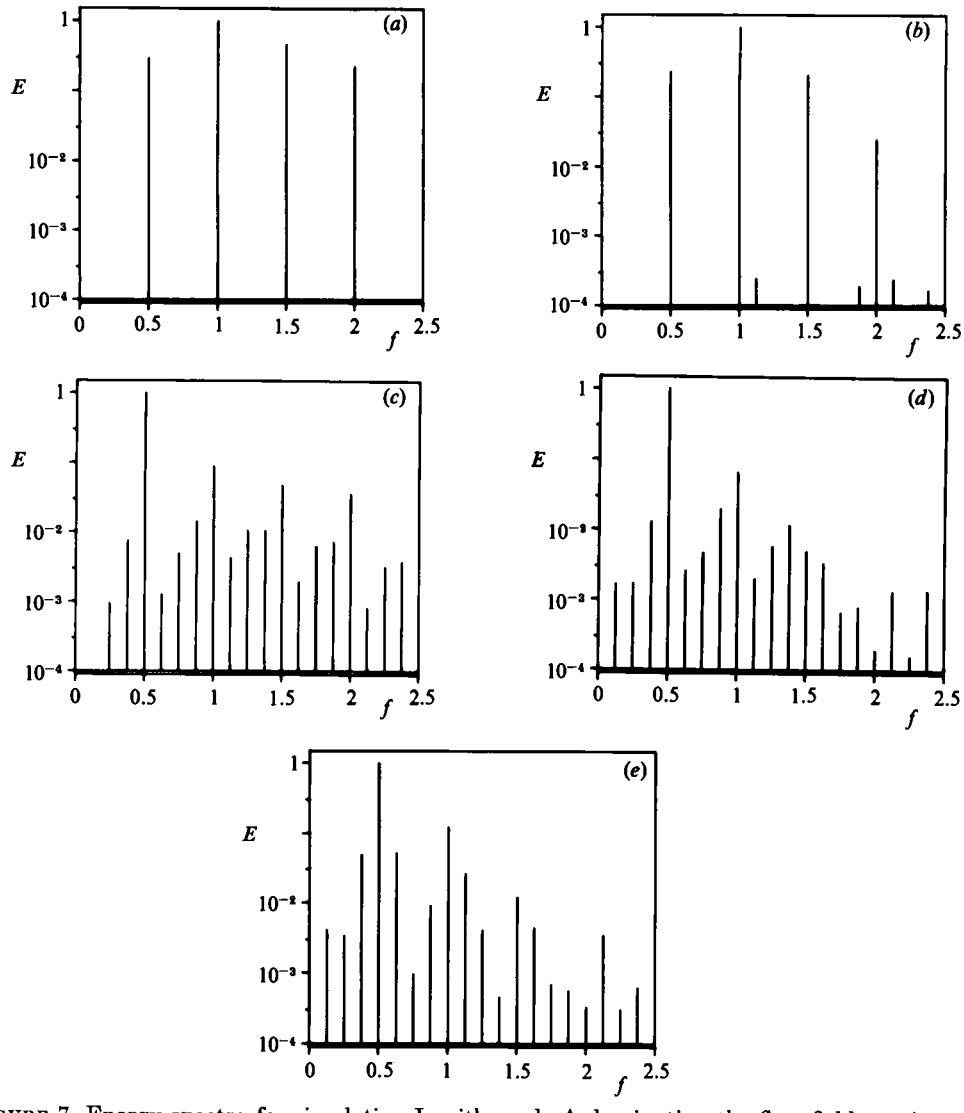

FIGURE 7. Energy spectra for simulation I, with mode A dominating the flow field, at times (*a*) $t = 34.4$, (*b*) 159.4, (*c*) 346.9, (*d*) 471.9, (*e*) 596.9. $f = 1$ is the frequency of the basic wave, $f = 0.5$ denotes the subharmonic wave. Initially the amplitude of the basic frequency experiences the strongest growth, but later most of the energy is contained in the subharmonic peak.

The fact that the v-velocity signal is still being recorded at the same position as in simulation I, is responsible for variations in the amplitudes of the various frequencies.

The above computational results indicate that the forced vortex street can change its lengthscale as a consequence of the pairing process. The numerical simulations also confirm the existence of two modes leading to opposite developments of the pairing transition.

In order to find out how a vortex street develops if both modes appear we have carried out simulation III. The control volume now contains 24 basic wavelengths and each layer is represented by 2365 discrete vortex blobs. The initial subharmonic disturbance, which now has an amplitude of 0.2, is constant throughout the control

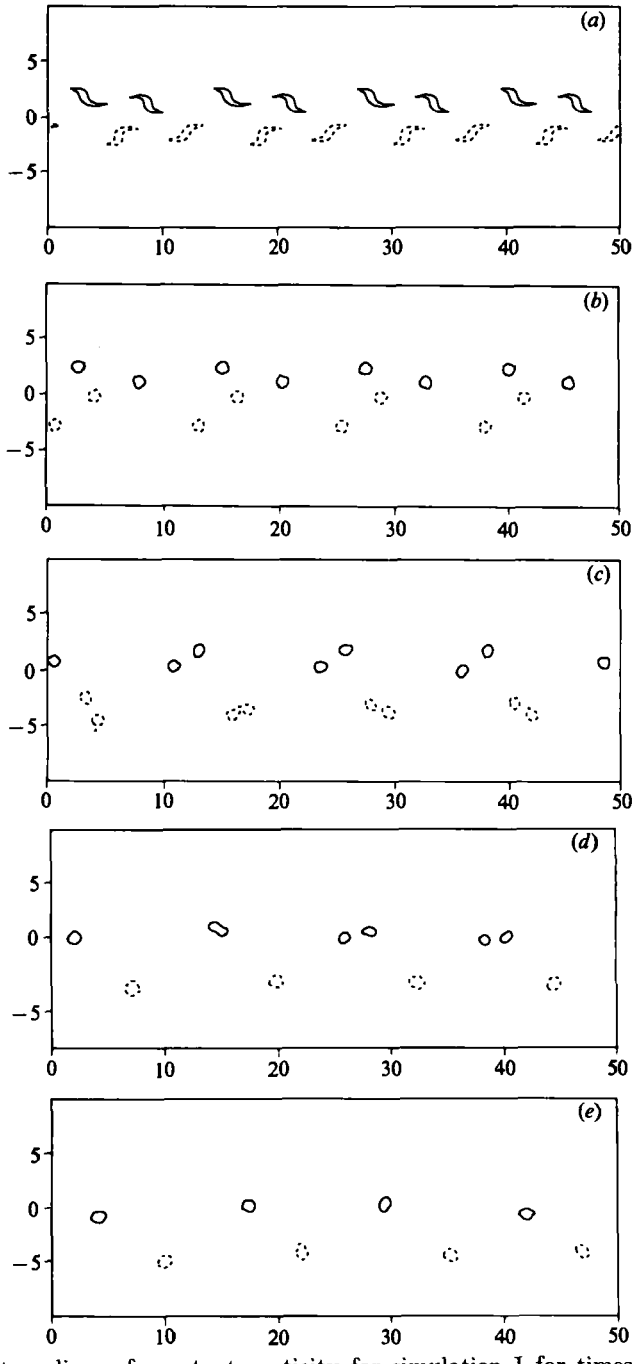

FIGURE 8. Contour lines of constant vorticity for simulation I for times as for figure 7. The subharmonic perturbation initially grows faster in the upper row, but later the pairing process is first completed in the lower row.

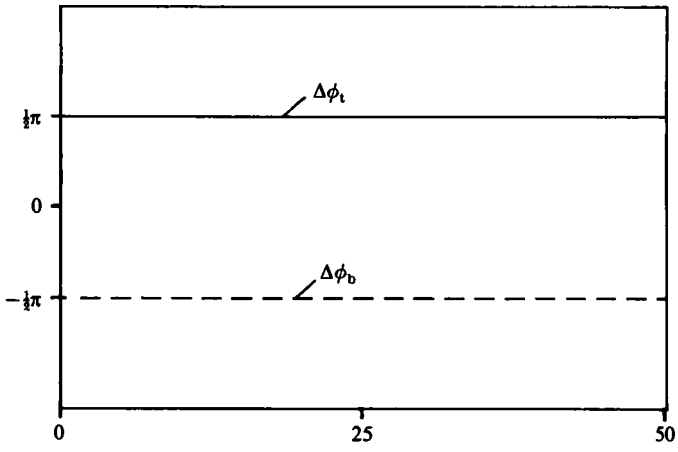

FIGURE 9. The phase relations of the subharmonic perturbations in the upper and the lower layer *vs.* the streamwise coordinate (simulation II).

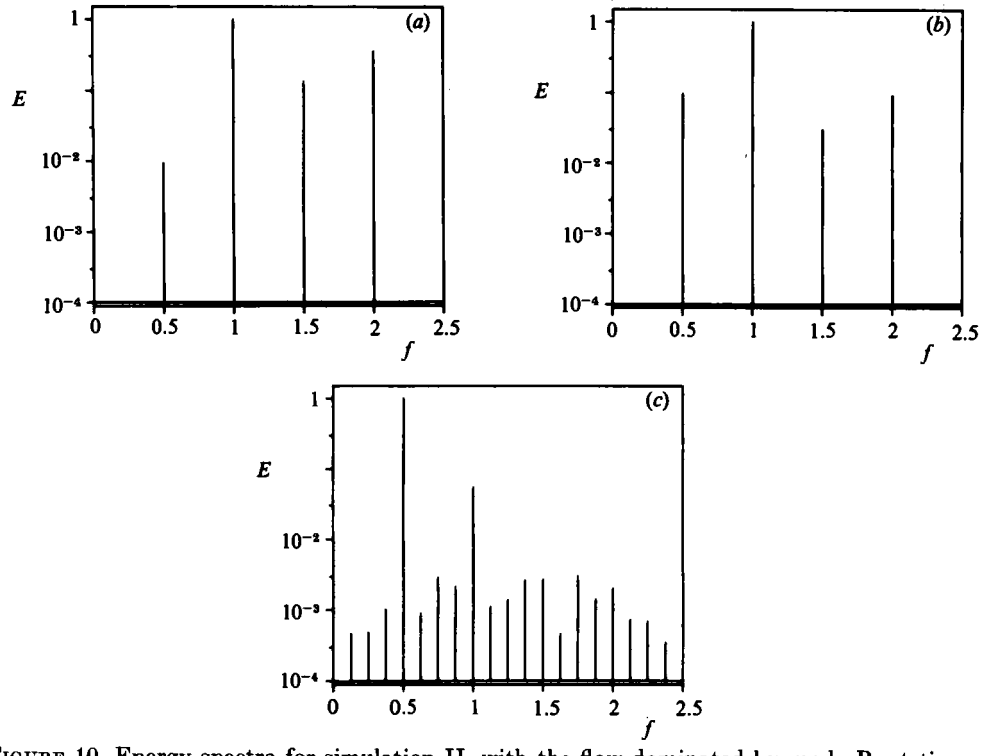

FIGURE 10. Energy spectra for simulation II, with the flow dominated by mode B, at times (*a*) $5 = 34.4$, (*b*) 96.9, (*c*) 471.9. The spectra show no principal differences compared to those of mode A.

volume for the upper row and has a phase difference $\Delta\phi_t$ of $\frac{1}{2}\pi$. In the lower layer periods 5–12 ($x = 25.13$ to 75.40) are now subject to the subharmonic perturbation with a phase difference $\Delta\phi_b$ of $\frac{1}{2}\pi$ and periods 17–24 ($x = 100.53$ to 150.80) are subject to a subharmonic wave of phase difference $\Delta\phi_b = \frac{1}{2}\pi$ (figure 12). This means that we should expect mode A in the region containing periods 5–12 and mode B in the region of periods 17–24. In the energy spectrum (figure 13) this is initially reflected by the

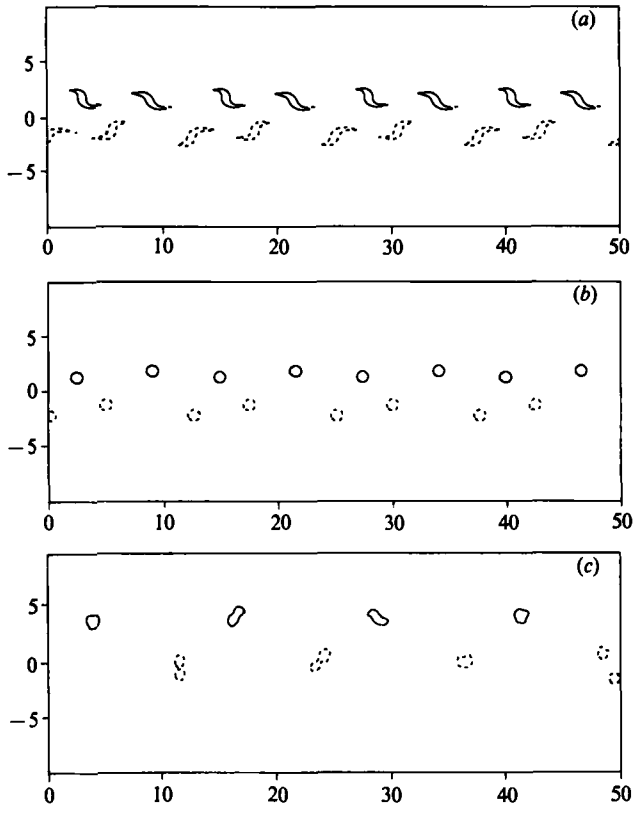

FIGURE 11. Vorticity contours of flow simulation II. Times as for figure 10. The development of the vortex street now proceeds in a manner opposite to simulation I.

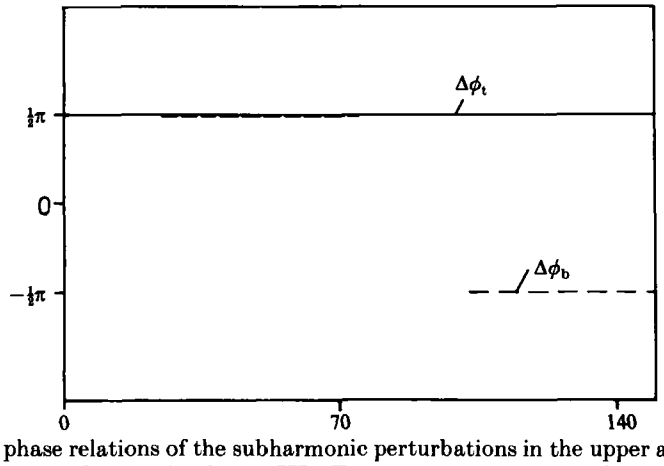

FIGURE 12. The phase relations of the subharmonic perturbations in the upper and the lower layer *vs.* the streamwise coordinate (simulation III). From $x = 25.13$ to 75.40 they correspond to mode A, whereas from $x = 100.53$ to 150.80 they represent mode B.

appearance of odd multiples of a small frequency $f_1 = \frac{1}{24}$ describing the periodicity of the whole flow field with the control volume. The nonlinear development, however, causes the even multiples to be excited as well. The peak denoting the subharmonic wave is due to the subharmonic perturbation of the upper row only. The subharmonic

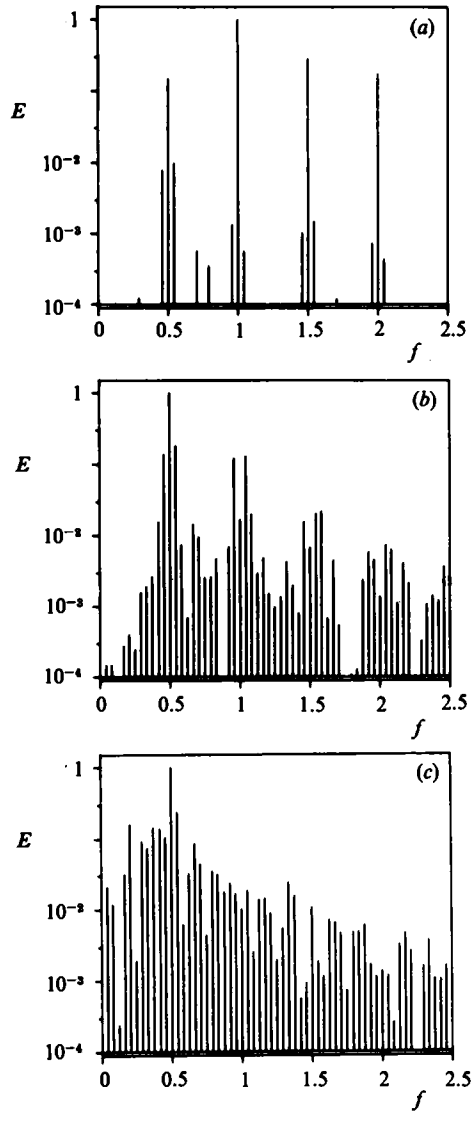

FIGURE 13. Energy spectra for simulation III at times (*a*) $t = 26.3$, (*b*) 213.8, (*c*) 631.3. In addition to the basic and the subharmonic frequency, the multiples of a small frequency f_1 describing the periodicity of the whole flow field are amplified. Again the maximum energy shifts from the basic to the subharmonic frequency in the course of the simulation.

disturbance of the lower layer does not cause the subharmonic frequency to appear in the spectrum as long as the numbers of wavelengths with opposite phase relations are equal. The envelope of the peaks of the small frequency and its multiples, however, has its maximum close to the wavelength dominating within each of the subharmonic wavetrains, i.e. close to $f = 0.5$.

At the beginning of the calculation the basic wavelength again experiences the strongest amplification (figure 14). Soon configurations form in the different regions of the flow field that correspond to those observed in the above simulations, so that each mode dominates a different part of the flow. This is again reflected by the fact that the subharmonic frequency and multiples of the small frequency f_1 close to it develop the highest amplitudes, whereas the energy of the basic wave decreases. It

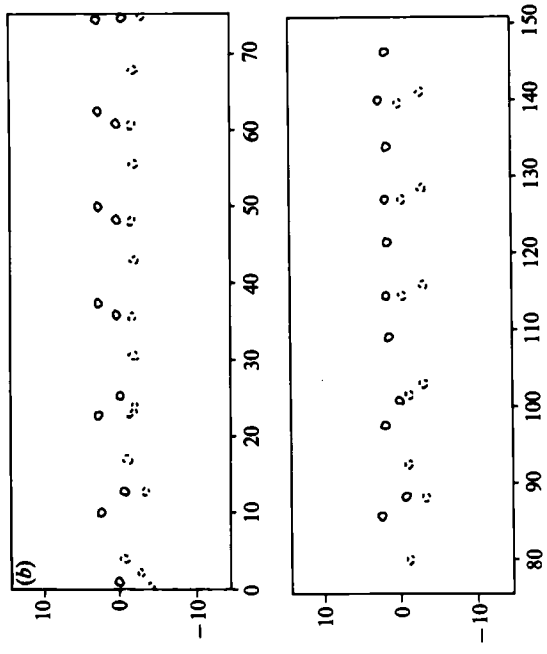

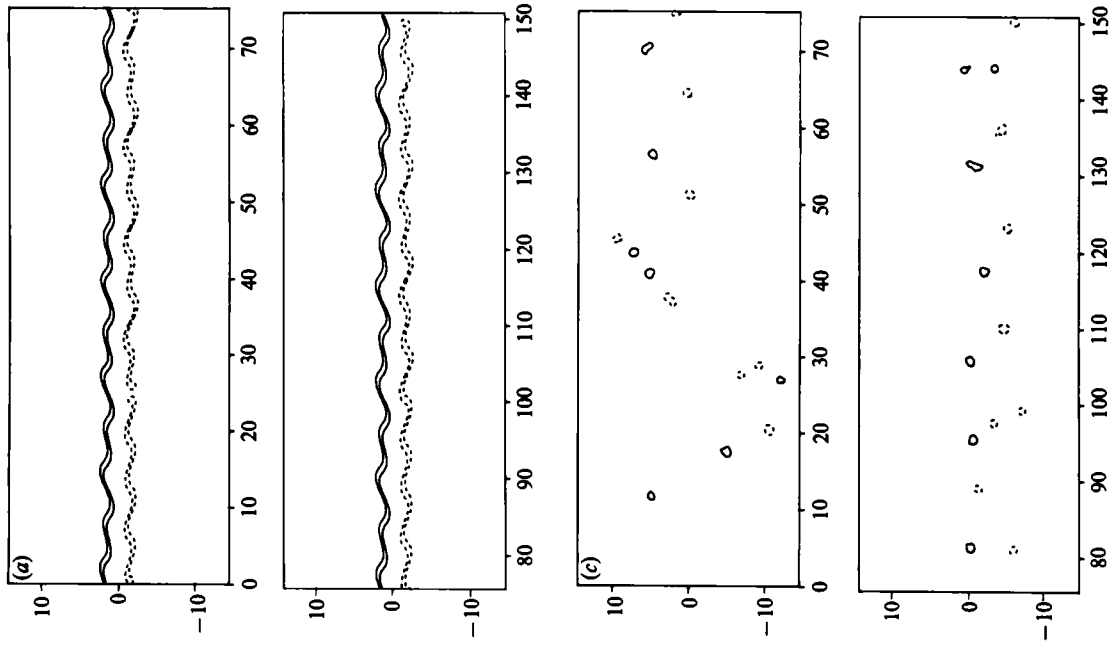

FIGURE 14. Vorticity contour plots for simulation III. Times are as figure 13. From (*b*), $t = 213.8$, we observe that the development of those regions initially containing subharmonic perturbations of mode A or B, respectively, proceeds according to simulations I and II. On (*c*), $t = 631.3$, we see regular regions from $x \approx 50$ to 70 and from $x \approx 105$ to 140 in which the vortex street has changed its lengthscale as a consequence of a pairing transition.

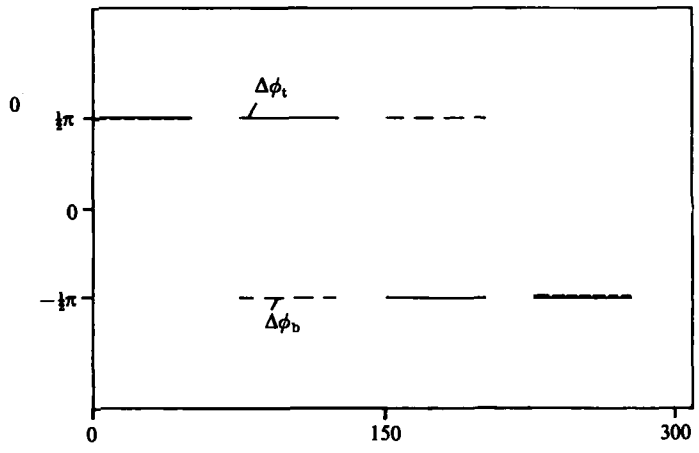

FIGURE 15. The phase relations of the subharmonic perturbations in the upper and the lower layer *vs.* the streamwise coordinate (simulation IV). These disturbances correspond to mode A from $x = 0$ to 50.27 and from $x = 226.19$ to 276.46, whereas they represent mode B from $x = 75.40$ to 125.66 and $x = 150.80$ to 201.06.

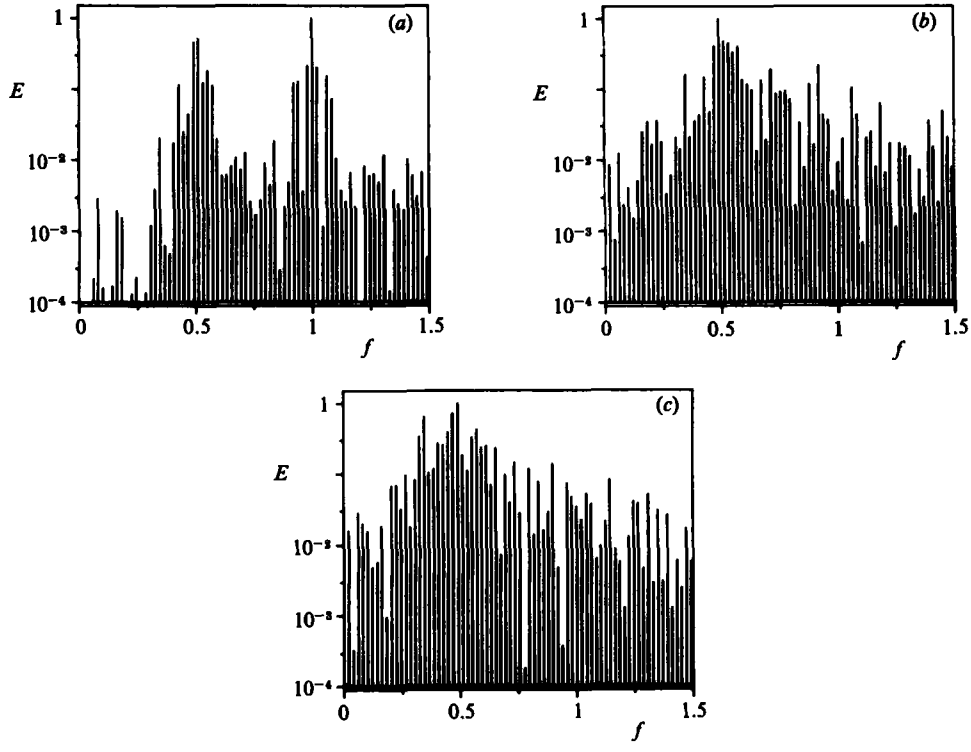

FIGURE 16. Energy spectra for simulation IV. Note that owing to the cancellation effect of subharmonic waves with different phase values the subharmonic peak does not show up. Besides the basic frequency $f_k = 1$ the small frequency $f_1 = f_k/49$ representing the periodicity of the whole flow field and its multiples are excited. In the course of the calculation the energy shifts from f_k to the peaks of those multiples of f_1 located in the neighbourhood of $\frac{1}{2}f_k$.

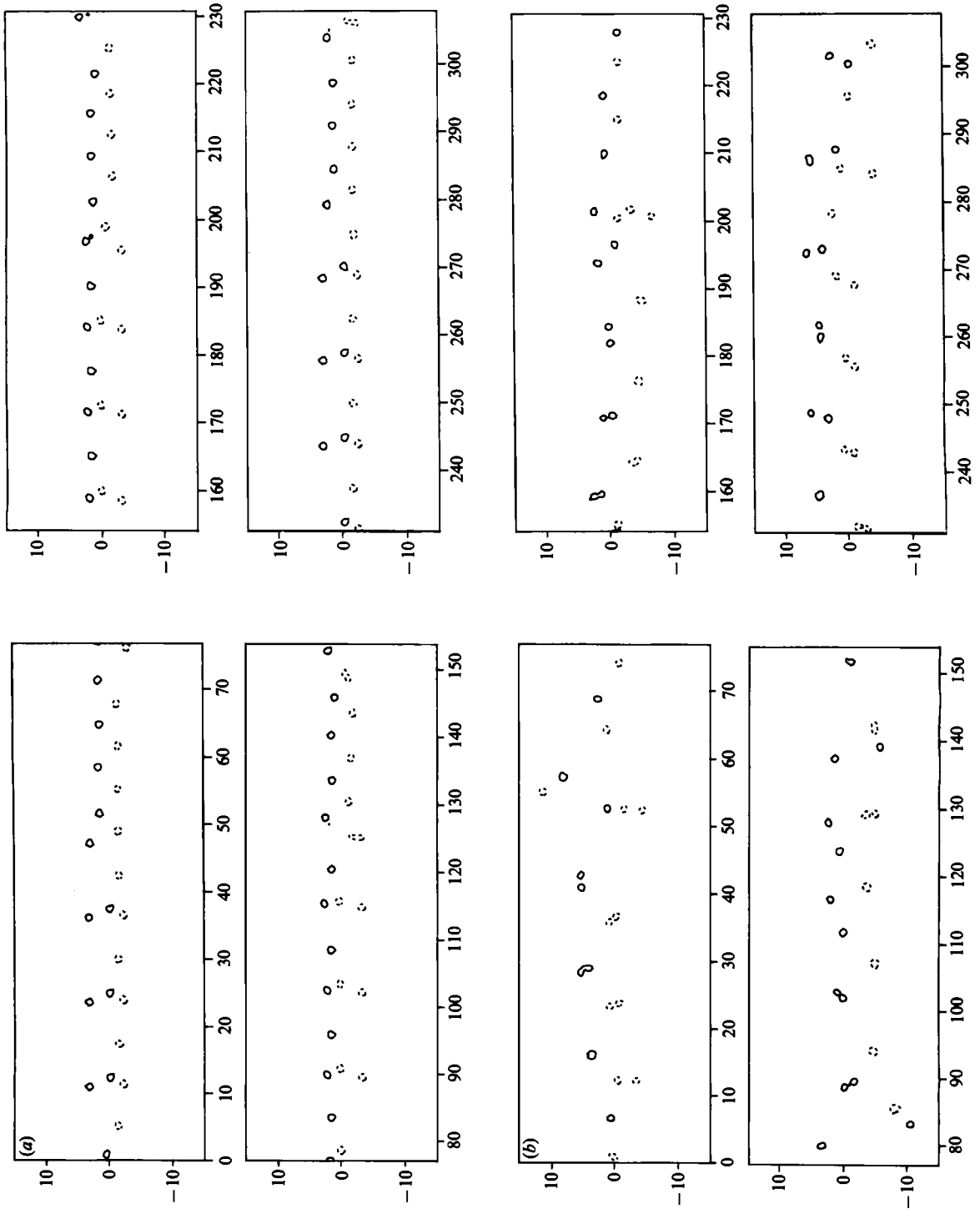
(a)
(b)
10
0
−10
0 10 20 30 40 50 60 70
80 90 100 110 120 130 140 150
160 170 180 190 200 210 220 230
240 250 260 270 280 290 300

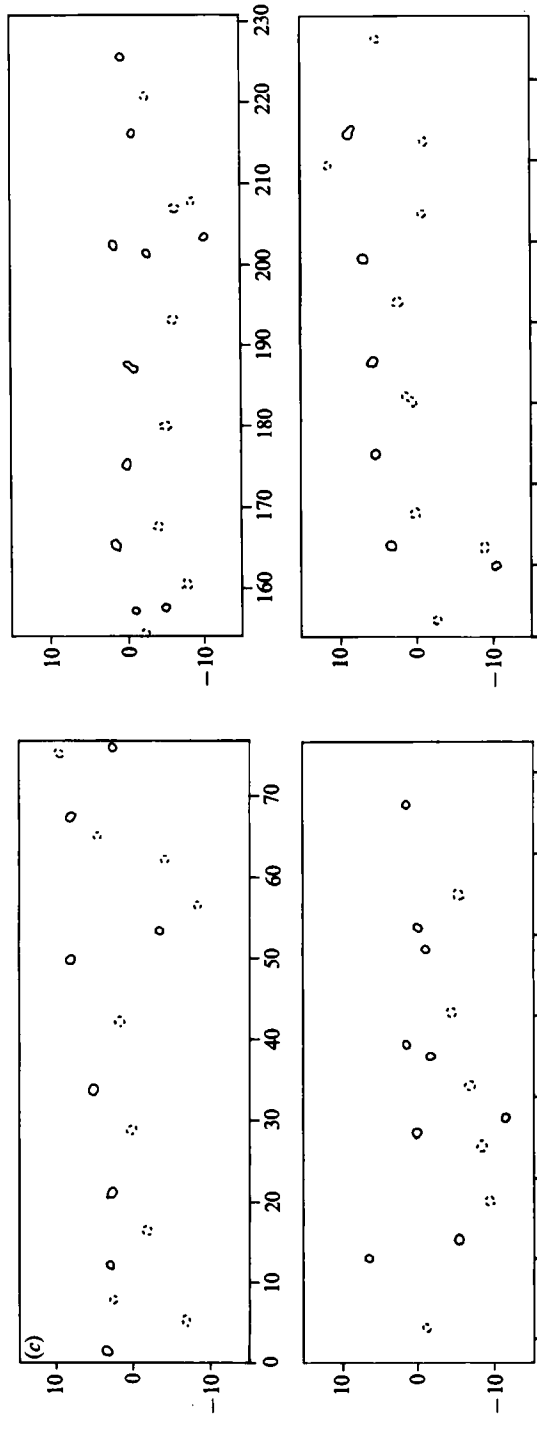

FIGURE 17. Vorticity contour lines for simulation IV at times (*a*) $t = 188.8$, (*b*) 488.8, (*c*) 727.2. The regions initially perturbed by subharmonic waves experience a regular development corresponding to the respective modes. In (*c*), those regions have undergone a pairing transition. The vortex street has consequently changed its lengthscale and rearranged itself into a larger one as can be observed in the regions from $x \approx 15$ to 50, from $x \approx 120$ to 150, from $x \approx 165$ to 195, and from $x \approx 245$ to 280.

becomes obvious that the presence of subharmonic perturbations with different phase relations can lead to the appearance of groups within which the lengthscale of the vortex street increases as a consequence of vortex pairing.

A real flow with purely random perturbations should contain subharmonic waves with all phase values both in the upper and in the lower layer. If averaged over a large number of basic wavelengths, the number of wavelengths with opposite phase relations should be approximately equal. In order to simulate this case we have carried out simulation IV, which contains both kinds of subharmonic waves in both the upper and the lower layer (figure 15). The control volume now contains a total of 49 wavelengths, each discretized into 91 vortex blobs in each layer. In the upper layer the subharmonic has the phase difference $\Delta\phi_t = \frac{1}{2}\pi$ for periods 1–8 ($x = 0$ to 50.27) and 13–20 ($x = 75.40$ to 125.66), and $-\frac{1}{2}\pi$ for periods 25–32 ($x = 150.80$ to 201.06) and 37–44 ($x = 226.19$ to 276.46). The lower layer is initially perturbed by a subharmonic wave of $\Delta\phi_b = \frac{1}{2}\pi$ for periods 1–8 and 25–32 and by one of $\Delta\phi_b = -\frac{1}{2}\pi$ for periods 13–20 and 37–44. This way the four possible combinations of the upper and lower subharmonic waves occur with each combination being confined to a region of eight basic wavelengths. These four regions are separated by transitional regions in which initially only the basic perturbation is present. Since in each layer the numbers of wavelengths with opposite phase relations are equal, the subharmonic peak in the frequency spectrum is not excited (figure 16). The small frequency and its multiples that appear in the spectrum reflect the periodicity of the flow field with the control volume. We recognize that again in the regions dominated by one of the modes a very regular vortex pairing process takes place which leads to the growth and a change in the lengthscale of the vortex street (figure 17). In the regions where the transition from one mode to the other occurs the structure appears to be rather irregular, and a specific pattern is not recognizable. Here a pairing of two like-signed vortices can happen as well as the formation of a neutral dipole consisting of two opposite-signed vortices. This strongly nonlinear behaviour observed in the transition regions might be related to the fact that they are rather short and that at the border between a transitional region and a region dominated by one of the modes the amplitude of the subharmonic wave does not increase smoothly but in the form of a step function.

4. Discussion

The results of the inviscid calculations presented above suggest that vortex pairing is able to account for the growth of the vortex street. At the same time it becomes obvious that, if individual subharmonic perturbations of each side of the wake are responsible for the pairing, the subharmonic frequency does not have to play a prominent role in the spectrum. Instead, the possible alternating existence of two subharmonic modes, which dominate different parts of the flow field, can lead to the appearance of a small frequency and its multiples. While the two subharmonic modes cause a cancellation of the subharmonic peak in the spectrum, the envelope of the multiples of the small frequency is expected to have its maximum close to the subharmonic peak.

The hypothesis of two different subharmonic modes dominating different parts of the flow field is supported by the experimental observation of a group structure of the far wake by Townsend (1979) and Cimbala (1984). They find that these groups have different frequencies, but the fact that within each group the frequency remains constant underlines their regular structure.

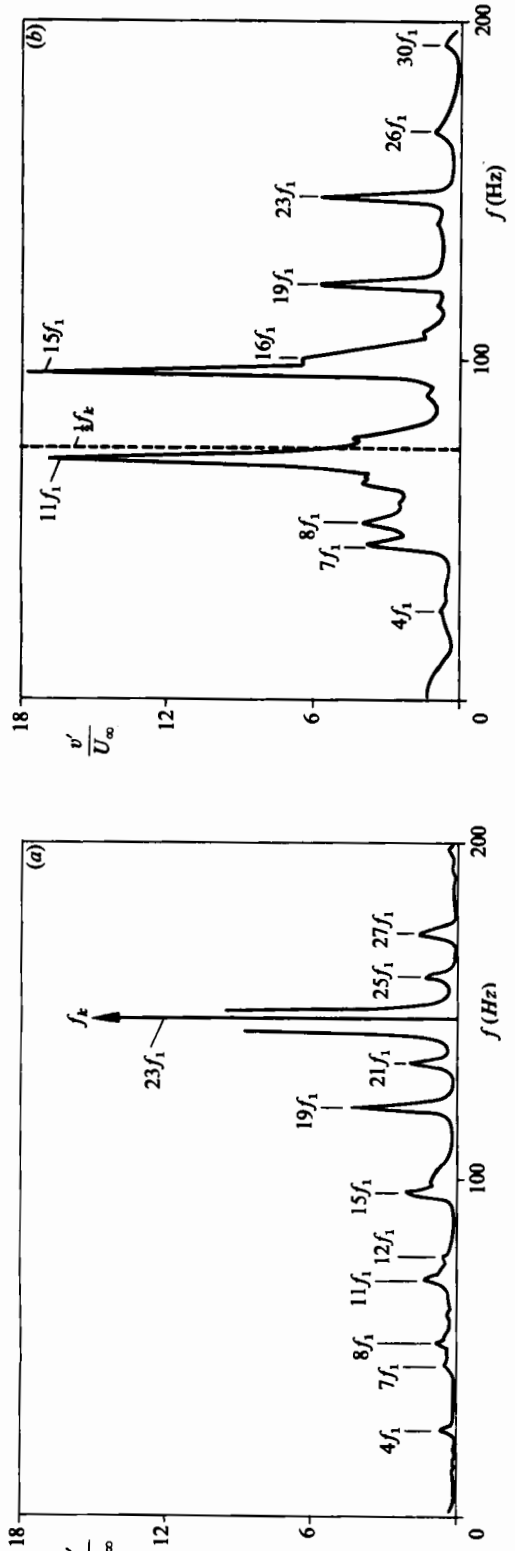

FIGURE 18. Frequency spectrum in the far wake of a circular cylinder of diameter d for $Re = 140$ as recorded by Cimbala (1984). (*a*) At $x/d = 40$ almost all peaks can be interpreted as multiples of $f_1 \approx 6.41$ Hz. The highest peaks occur close to the shedding frequency f_k. (*b*) At $x/d = 100$ the highest peaks (still multiples of f_1) occur in the neighbourhood of the subharmonic of f_k. (*c*) At $x/d = 350$ the highest peaks show up close to the second subharmonic of f_k. The discrete peaks still represent multiples of $f_1 \approx 6.41$ Hz.

If we compare our numerical results in more detail with the experiments carried out by Cimbala (1984) for a Reynolds number of 140 we find a number of common features. An analysis of his figure 5.5 (figure 18) shows that by $x/d = 40$ discrete frequencies have appeared, predominantly close to the shedding frequency. In this case, d denotes the diameter of the cylinder that was used to generate the wake. As far as we can conclude from the resolution provided by the figures given in Cimbala's report, all these frequencies can be explained as multiples of a small frequency of about 6.41 Hz, which could be taken as evidence for the formation of a very regular group structure. It is unknown at present, however, what could be the reason for such a strong periodicity of the groups. Acoustic effects might play a role here, i.e. a feedback loop might exist similar to the case investigated by Koshigoe, Yang & Culick (1985) for the single shear layer. If the group structure is the reason for the emergence of the discrete frequencies, the fact that most of the peaks are located close to the shedding frequency indicates that at this position the pairing process within the groups has not yet proceeded very far, so that within the groups the shedding frequency still dominates. At $x/d = 100$ Cimbala also observes discrete frequencies which do not contain the subharmonic itself but show the highest peaks in its neighbourhood. They can again be interpreted as multiples of the small frequency of 6.41 Hz. In the light of our very similar numerical results this could mean that the pairing process now has experienced considerable amplification within the groups. At $x/d = 350$ the peaks of the discrete frequencies have shifted to the proximity of the second subharmonic, and they can still be expressed in terms of multiples of the same small frequency. This could indicate a second pairing transition within the groups.

Cimbala's experiments for $Re = 150$ (figure 19) also seem to support the considerations presented here. Some of the discrete frequencies can be interpreted as multiples of the small frequency of about 16.6 Hz. At $x/d = 100$ the highest peaks have again shifted to the neighbourhood of the subharmonic frequency, and at $x/d = 200$ they cluster around the subharmonic even more clearly. But not all of the discrete frequencies can be expressed in terms of multiples of one basic frequency as was the case for $Re = 140$. This might be related to the fact that at $Re = 150$, which is closer to the transition to turbulence, the periodicity of the flow has deteriorated, so that groups of different lengths could have appeared, which would cause the spectrum to develop a more complicated structure. Frequency spectra of finer resolution would certainly be helpful for a more detailed investigation.

In the light of the above discussion the very regular vortex pairing observed by Matsui & Okude (1983) in the forced wake now appears logical since the forcing prevents the existence of two different modes. Matsui & Okude's photographs also reveal that the two sides of the wake proceed towards a pairing at different speeds, which confirms our above analysis of the different growth rates of the respective subharmonic perturbations of the two rows of vortices.

The appearance of two competing subharmonic modes might also be the reason for the breakdown of the two-dimensional temporally amplified vortex street analysed by Aref & Siggia (1981). In their figure 12 the random perturbations are of such a nature that in the lower row vortices A and B, and E and F do pair (initially C and D also seem to proceed towards a pairing), while in other parts of the flow field none of the modes seems to dominate.

The assumption of almost inviscid dynamics presents a major limitation of our work. Viscous effects might play a significant role in the evolution of the far-wake structure, especially for low Reynolds numbers, and they should be included in future

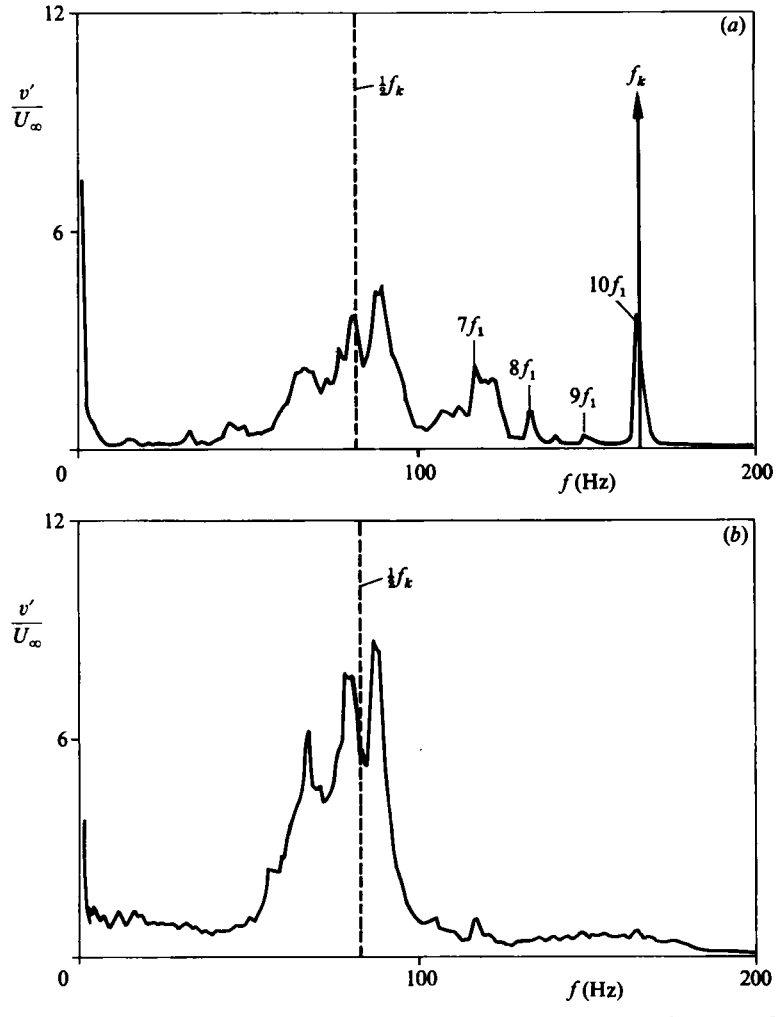

FIGURE 19. Frequency spectrum in the far wake of a circular cylinder of diameter d for $Re = 150$ as recorded by Cimbala (1984). (*a*) At $x/d = 100$ a number of peaks can be interpreted as multiples of $f_1 \approx f_k/10$. Some of the highest peaks occur close to the shedding frequency f_k, whereas others cluster around its subharmonic. By comparison with the spectra for $Re = 140$ we find that the periodicity of the flow has deteriorated and that we can no longer express all peaks in terms of f_1. (*b*) At $x/d = 200$ the highest peaks occur in the neighbourhood of the subharmonic of f_k.

numerical studies. At this point we can only make a few tentative suggestions as to the influence of viscosity. In the transitional regions between the groups viscous effects can lead to the cancellation of vortices of opposite signs, thus resulting in the loss of some of the individual vortex structures. One could imagine that upon this cancellation of vorticity in the transitional regions, which is expected to become more significant as the Reynolds number decreases, the regular structure of the neighbouring regions might slightly change its wavelength and 'fill up' part of the transitional region, thus causing the new lengthscale of the vortex street not to be exactly twice the old one but slightly larger. This way viscous effects could influence the ratio of the lengthscales of the secondary and the primary vortex streets. Decreasing influence of viscous forces thus would result in a lower ratio of these lengthscales. This points in the same direction as Taneda's (1959) observations. In

the Reynolds number regime $50 < Re < 150$ he found this ratio to decrease from slightly above 3 to about 2. The loss of individual structures in the transitional region by viscous effects together with the subsequent extension of the regular region could also be related to Cimbala's (1984) observation that the frequency of the secondary vortex street varies from group to group.

Our argumentation so far has been purely two-dimensional, but the existence of different modes along with viscous effects can also be of importance for the spanwise structure of the flow field. Just as different subharmonic disturbances have an opposite influence on the development of the flow at varying streamwise positions, the same can be the case in the spanwise direction. This could lead to a configuration in which the spanwise vortex B might pair with A at one spanwise position and with C at another position, with a consequent transitional region in between. Here viscous forces might again have the effect of cancellation of some of the vorticity of opposite signs, thus possibly leading to changes in the topological structure. The relinking of the vortices could cause the formation of vortex loops, about which there has been some speculation in the literature (see Roshko 1976). In this respect the wake would behave fundamentally differently from the single shear layer where only one sign of vorticity is present. This could be related to observations by Breidenthal (1980) which indicate that the wake is more sensitive to variations in the spanwise direction than the single shear layer. It should be emphasized, however, that at present all the possible consequences related to viscous and three-dimensional effects are speculative. Future investigations should include further experiments as well as viscous and three-dimensional calculations in order to clarify to what degree the stability characteristics of the average wake profile and the process of vortex pairing are responsible for the change of the lengthscale of the unforced wake flow.

The author wishes to express sincere thanks to Dr W. T. Ashurst for discussions on both the numerical and the physical aspects of the problem under consideration.

REFERENCES

AREF, H. & SIGGIA, H., 1981 Evolution and breakdown of a vortex street in two dimensions. *J. Fluid Mech.* **109**, 435–463.

BREIDENTHAL, R. 1980 Response of plane shear layers and wakes to strong three-dimensional disturbances. *Phys. Fluids* **23**, 1929–1934.

CIMBALA, J. M. 1984 Large structure in the far wakes of two-dimensional bluff bodies. Ph.D. thesis, California Institute of Technology.

CORCOS, G. M. & SHERMAN, F. S. 1984 The mixing layer: deterministic models of a turbulent flow. Part 1. Introduction and the two-dimensional flow. *J. Fluid Mech.* **139**, 29–65.

KOCH, W. 1985 Local instability characteristics and frequency determination of self-excited wake flows. *J. Sound Vib.* **99**, 53–83.

KOSHIGOE, S., YANG, V. & CULICK, F. E. C. 1985 Calculations of interaction of acoustic waves with a two-dimensional free shear layer. *AIAA paper* 85-0043.

LAMB, H. 1932 *Hydrodynamics*, 6th edn. Cambridge University Press.

LEONARD, A. 1980 Vortex methods for flow simulation. *J. Comp. Phys.* **37**, 289–335.

LEONARD, A. 1985 Computing three-dimensional incompressible flows with vortex elements. *Ann. Rev. Fluid Mech.* **17**, 523–559.

MATSUI, T. & OKUDE, M. 1983 Formation of the secondary vortex street in the wake of a circular cylinder. In *Structure of Complex Turbulent Shear Flow, IUTAM Symposium, Marseille, 1982* (ed. R. Dumas & L. Fulachier). Springer.

MEIRON, D. I., SAFFMAN, P. G. & SCHATZMAN, J. C. 1984 The linear two-dimensional stability of inviscid vortex streets of finite-cored vortices. *J. Fluid Mech.* **147**, 187–212.

PATNAIK, P. C., SHERMAN, F. S. & CORCOS, G. M. 1976 A numerical simulation of Kelvin–Helmholtz waves of finite amplitudes. *J. Fluid Mech.* **73**, 215–240.

RILEY, J. J. & METCALFE, R. W. 1980 Direct numerical simulation of a perturbed, turbulent mixing layer. *AIAA paper* 80-0274.

ROSHKO, A. 1976 Structure of turbulent shear flows: a new look. *AIAA J.* **14**, 1349–1357.

SIROVICH, L. 1985 The Kármán vortex trail and flow behind a circular cylinder. *Phys. Fluids* **28**, 2723–2726.

TANEDA, S. 1959 Downstream development of the wakes behind cylinders. *J. Phys. Soc. Japan* **14**, 843–848.

TOWNSEND, A. A. 1979 Flow patterns of large eddies in a wake and in a boundary layer. *J. Fluid Mech.* **95**, 515–537.

WINANT, C. D. & BROWAND, F. K. 1974 Vortex pairing: the mechanism of turbulent mixing layer growth at moderate Reynolds number. *J. Fluid Mech.* **63**, 237–255.